NASA
Technical
Paper
2955
C.2

November 1989

Emittance, Catalysis, and Dynamic Oxidation of Ti-14Al-21Nb

K. E. Wiedemann,
R. K. Clark, and
S. N. Sankaran

NASA

NASA Technical Paper 2955

1989

Emittance, Catalysis, and Dynamic Oxidation of Ti-14Al-21Nb

K. E. Wiedemann
Analytical Services & Materials, Inc.
Hampton, Virginia

R. K. Clark
Langley Research Center
Hampton, Virginia

S. N. Sankaran
Analytical Services & Materials, Inc.
Hampton, Virginia

NASA
National Aeronautics and Space Administration
Office of Management
Scientific and Technical Information Division

Symbols

c_1	first radiation constant, 3.7415×10^{-16} W/m^2
c_2	second radiation constant, 1.43879×10^{-2} m-K
c_c	heat capacity of the ceramic insulator, J/kg-K
c_e	mole fraction of atomic air
c_m	heat capacity of the metal specimen, J/kg-K
C	composition, atom percent
C_0	initial composition, atom percent
C_S	surface composition, atom percent
D	diffusion coefficient, cm^2/sec
f	compositional broadening spectrum, counts/sec-deg
g	instrumental plus sample-defect broadening spectrum, counts/sec-deg
h_R	specific enthalpy of recombination, J/kg
h_{se}	specific free-stream enthalpy, J/kg
K_c	thermal conductivity of the ceramic insulator, W/cm-K
l	depth, cm
L_c	thickness of the ceramic insulator, m
L_m	thickness of the metal specimen, m
M_A	mass of atomic air, g
M_λ	Planck's radiation function, W/m^2-μm
P_0	incident power, counts/sec
p_{se}	stagnation pressure, atm
q_{aero}	aerodynamic heating, W/m^2
q_c	convection component of aerodynamic heating, W/m^2
q_{cond}	heat loss by conduction, W/m^2
q_D	potential heating due to recombination of gaseous atoms, W/m^2
q_{rad}	heat loss by radiation, W/m^2
Q	linear reflectivity, cm^{-1}
R	universal gas constant, 8.31441 J/mole-K
s	compositional plus instrumental and sample-defect broadening spectrum, counts/sec-deg
Sc	Schmidt number
t	time, sec
T	temperature, K
T_0	initial temperature, K
T_w	wall temperature at the stagnation point

β	velocity gradient in boundary layer, sec^{-1}
γ	catalytic efficiency
δ	d-spacing, Å
δ_0	d-spacing of the surface composition
ϵ_T	total hemispherical emittance
ϵ_λ	spectral emittance
κ_b	Lagrange multiplier for background constraint
κ_s	Lagrange multiplier for smoothing constraint
λ	wavelength
μ	linear absorption coefficient, cm^{-1}
μ_{se}	viscosity of gases at the stagnation point in the boundary layer, g/cm-sec
ρ_c	density of the ceramic insulator, g/cm^3
ρ_m	density of the metal specimen, g/cm^3
ρ_{se}	density of gases at the stagnation point in the boundary layer, g/cm^3
ρ_w	density of gases at the specimen surface, g/cm^3
ρ_λ	spectral reflectance
σ	Stefan-Boltzmann constant, 5.6697×10^{-8} W/m^2-K^4
$\bar{\sigma}$	Prandtl number
υ	background compositional broadening spectrum constraint
ϕ_γ	recombination factor
Ψ	modified diffracted power, counts/sec/deg

Summary

Emittance, catalytic efficiency, and dynamic oxidation resistance were determined for Ti-14Al-21Nb exposed to simulated hypersonic flight conditions at a surface temperature of 982°C for up to 8 hr. The emittance was low before testing (about 0.3), but high after testing (0.85 to 0.89). Catalytic efficiencies were high, which means that during exposure to hypersonic conditions Ti-14Al-21Nb will experience a large amount of heating due to recombination of gaseous atoms at the surface. Oxides that formed on the surface spalled readily, beginning with the first exposure cycle. Oxygen diffusion into the base metal was observed. The solubility limit of oxygen in the base metal was estimated to be 12.5 atom percent, and the diffusion coefficient for oxygen in the base metal was 0.0234 $cm^2/sec\ \exp\left(\frac{-45\,090\ cal/mole-K}{RT}\right)$ between 704°C and 982°C (where R is the universal gas constant and T is the absolute temperature). The oxide was composed of several layers of different color but similar composition: TiO_2, Al_2O_3, TiN, and Ti_3O_5 were identified by X-ray diffraction.

Introduction

Ti-14Al-21Nb is a purportedly ductile modification of the titanium aluminide Ti_3Al; titanium aluminides are intermetallics offering improved performance for hypersonic vehicles over conventional superalloys and titanium because of higher strengths and lower densities. In addition to high strength and low density, materials for hypersonic applications must be resistant to the dynamic oxidation resulting from forced flowing air of hypersonic flight, must radiate heat well (high emittance), and must experience a minimum of heating from recombination of gaseous atoms at the surface (low catalytic efficiency).

In a given hypersonic environment, the temperature of a vehicle surface is determined by the material properties emittance and catalytic efficiency. The optimum values of emittance and catalysis are 1 and 0, respectively. Calculations showing the variation in surface temperature with emittance and catalytic efficiency are presented in figure 1. This represents a modest environment for which the catalytic heating effects are not severe, yet the surface temperature can range from 800° to 1400°C. Under more severe conditions the effect of catalytic heating is more critical (ref. 1).

Some materials that may be very stable under static conditions oxidize much more rapidly under hypersonic conditions because of the atomic oxygen environment and low atmospheric pressures where sublimation and formation of gaseous oxides may readily occur. For metallic materials the key to durability is formation of an oxide layer that is protective and that, if the metal is susceptible to oxygen embrittlement, blocks the transport of oxygen into the alloy. While oxygen embrittlement has not yet been demonstrated for Ti-14Al-21Nb, it has for α-titanium, which is closely related in chemistry and crystal structure.

The purpose of this study was characterization of Ti-14Al-21Nb performance under simulated hypersonic conditions. Specimens were exposed to simulated hypersonic flight (dynamic oxidation conditions) for 1 to 16 half-hour cycles at a surface temperature of 982°C. Analyses of heating rates were used to determine catalytic efficiency. Oxide composition and oxygen diffusion into the metal were observed with X-ray diffraction. Room temperature reflectance measurements were made to determine emittance. X-ray diffraction was performed on specimens exposed under static conditions to determine diffusion coefficients for oxygen in the alloy.

Experimental and Analytical Procedures

Test Specimens

The specimens were disks punched from 1-mm-thick sheet (the alloy composition is given in table I). The disks were 25 mm in diameter with three equally spaced 5- × 5-mm radial projections used for mounting.

Exposure of Specimens

Specimens were exposed to simulated hypersonic flight conditions in the hypersonic materials environmental test system (HYMETS) at the Langley Research Center (ref. 2). The HYMETS is a 100-kW constrictor-arc-heated wind tunnel that uses air mixed with nitrogen and oxygen in ratios equivalent to air (see fig. 2). Specimens were mounted on a stagnation model adapter attached to an insertion sting. A separate sting contained a water-cooled probe that measured the catalytic cold-wall heating rate and the surface pressure. The specimen temperature was monitored with a thermocouple (type R, attached at the center of the back surface).

The range of test conditions available in the HYMETS (table II) do not fully simulate hypersonic flight; however, the heating rate with high velocity air is the most critical response parameter, and the range of heating rate includes the levels encountered by a significant portion of a vehicle in hypersonic

flight. Chemical equilibrium calculations for the test conditions used in the present study indicate that oxygen in the test stream was almost fully dissociated (>95 percent) and nitrogen only slightly dissociated (<5 percent) (ref. 3).

Specimens were exposed to 1 to 16 half-hour cycles at 982°C. In each cycle, the specimen was first exposed to a reference test condition (table III), and its temperature history was recorded for the interval from ambient to about 75°C. The test condition was then adjusted to achieve a specimen surface temperature of 982°C for the balance of the cycle.

Emittance Study

Room temperature spectral reflectance measurements were made on specimens over the wavelength range of 1.5 to 25 μm using a Gier Dunkle Model HCDR 3 heated-cavity reflectometer (ref. 4).

The spectral radiant exitance of a blackbody is dependent on wavelength and temperature and is given by Planck's radiation function (ref. 5):

$$M_\lambda = \frac{c_1 \lambda^{-5}}{\exp[c_2/(\lambda T)] - 1} \tag{1}$$

Spectral emittance of a non-blackbody is the ratio of the spectral radiant exitance of the non-blackbody to the spectral radiant exitance of a blackbody. Spectral emittance is related to spectral reflectance by Kirchoff's Law (emittance equals absorptance at equivalent temperatures) and the relationship that absorptance equals unity minus reflectance (ref. 5), thus

$$\epsilon_\lambda = 1 - \rho_\lambda \tag{2}$$

The total emittance of a non-blackbody is defined by the equation (ref. 5)

$$\epsilon_T = \frac{\int_0^\infty \epsilon_\lambda M_\lambda \, d\lambda}{\int_0^\infty M_\lambda \, d\lambda} \tag{3}$$

The spectral emittance of most materials is independent of temperature when there are no significant changes in atomic structure. For a surface with no dependence of spectral emittance on temperature, the total emittance for any temperature can be calculated from spectral emittance data measured at another temperature by applying equation (3) with M_λ evaluated at the desired temperature.

Catalysis Study

The catalytic efficiency γ is defined as the fraction of atoms striking a surface that recombine. Catalytic efficiencies for surfaces can be determined from analysis of carefully measured aerothermal heating rates (refs. 1, 6, 7, and 8).

For conditions of aerothermal heat transfer to a surface with insulation at the back side, the heat transfer is described by

$$q_{\text{aero}} = \rho_m c_m L_m \frac{dT}{dt} + q_{\text{rad}} + q_{\text{cond}} \tag{4}$$

According to Goulard (ref. 1), the aerodynamic heating of a surface with a finite catalytic efficiency is given by

$$q_{\text{aero}} = q_c + q_D \, \phi_\gamma \tag{5}$$

where the convection heating is given by

$$q_c = 0.47 \sigma^{-2/3} (h_{se} - h_R c_e) \sqrt{2\beta \mu_{se} \rho_{se}} \tag{6}$$

and the potential heating due to recombination of gaseous atoms at the surface is given by

$$q_D = 0.47 Sc^{-2/3} h_R c_e \sqrt{2\beta \mu_{se} \rho_{se}} \tag{7}$$

The realized fraction of the potential heating due to recombination of gaseous atoms at the surface is given by

$$\phi_\gamma = \frac{1}{1 + \dfrac{0.47 Sc^{-2/3} \sqrt{2\beta \mu_{se} \rho_{se} R T_w}}{\gamma \rho_w \sqrt{2\pi M_A}}} \tag{8}$$

and, hence, the catalytic activity is given by

$$\gamma = \frac{0.47 Sc^{-2/3} \sqrt{2\beta \mu_{se} \rho_{se} R T_w}}{\left(\frac{1}{\phi_\gamma} - 1\right) \rho_w \sqrt{2\pi M_A}} \tag{9}$$

The radiant energy is given by the Stefan-Boltzmann equation:

$$q_{\text{rad}} = \epsilon_T \sigma T^4 \tag{10}$$

The conduction to the insulator is given by

$$q_{\text{cond}} = -K_c \frac{\partial T}{\partial x} \tag{11}$$

where

$$\rho_c c_c \frac{\partial T}{\partial t} + \frac{\partial}{\partial x}\left(K_c \frac{\partial T}{\partial x}\right) = 0 \tag{12}$$

For a brief time after inserting the specimen into the flow stream, the insulator can be treated as infinitely thick, and K_c as constant. Solving equation (12)

by using the method of Laplace transforms and the semi-infinite boundary condition gives

$$q_{\text{cond}} = -\frac{2}{\sqrt{\pi}} \sqrt{\rho_c c_c K_c (T - T_0) \frac{\partial T}{\partial t}} \qquad (13)$$

At steady state conditions, $\partial T/\partial t$ is zero, and integrating equation (12) yields

$$q_{\text{cond}} = -\frac{1}{L_c} \int_{T_{\text{back}}}^{T_{\text{front}}} K_c \, dT \qquad (14)$$

Diffusion Study

Very precise diffusion profile information can be determined by analysis of line broadening of diffraction spectra. To perform such an analysis it is necessary to isolate the compositional broadening component from the instrumental and sample-defect components. The spectra of a specimen that has no diffusion gradients is used to simultaneously determine the instrumental and sample-defect broadening. The compositional broadening is then extracted from the spectra of specimens that have diffusion gradients by solving (refs. 9 and 10):

$$g * f - s + (-1)^n \kappa_b (f^{2n} - v^{2n}) + (-1)^m \kappa_s f^{2m} = 0 \qquad (15)$$

where $g * f$ is the convolution of the f and g spectra, and the diffusion profile is given by (refs. 11 and 12)

$$l = \frac{\lambda}{2} \int_{\delta_0}^{\delta} \frac{f \, d\delta}{\delta Q (P_0 - \Psi)} \qquad (16)$$

where

$$\Psi = 2 \int_{\delta_0}^{\delta} \frac{\mu}{Q} \left[1 + (\mu\delta)^{-1} \frac{d\delta}{dx} \int_0^l \mu \, d\xi \right] f \, d\delta \qquad (17)$$

and composition is determined from the d-spacing by assuming that the lattice dilation of Ti-14Al-21Nb with dissolved oxygen content is the same as that of α-titanium (ref. 13).

Diffusion coefficients can be calculated from the profiles by using the relation

$$D = \frac{\pi}{4tC_S^2} \left\{ \int_{C_S}^{C_0} l[\delta(C)] \, dC \right\}^2 \qquad (18)$$

which assumes that the diffusion coefficient is independent of composition.

Results and Discussion

Dynamic Oxidation

Dynamic oxidation was marked by formation of an oxide layer, spalling of the oxide layer, and diffusion of oxygen into the metal. On some specimens spalling occurred during the first half-hour exposure cycle, which indicates that its cause was more likely the atomic oxygen environment or the low pressures than the thermal cycling. The oxide (see fig. 3) was composed of three layers having similar compositions: the top layer was white; the middle, grey; and the bottom, black. The white and grey layers were loosely adherent and readily spalled, but the black layer remained very adherent and never spalled.

Microstructure

The figure 4 micrographs show the changes that occurred during dynamic oxidation exposure. Before any exposure the microstructure was fine grained and, in X-ray diffraction (XRD) patterns, showed a (001) preferred orientation. After 8 hr of exposure, substantial changes in the microstructure occurred: an oxide layer formed, a portion of which is visible at the top of the micrograph; a new phase formed at the metal-oxide interface, which was identified by XRD and energy dispersive spectroscopy (EDS) as TiAl; a single-phase case developed below the TiAl; the base alloy recrystallized; and grain growth occurred in the base alloy. Comparing the micrograph of the sample after 8 hr exposure with micrographs for less exposure times showed the depth of the single-phase case to increase in proportion to the square root of time.

Diffraction Analysis

Analysis by XRD of the base alloy showed one structure, but with some peak splitting and some superlattice peaks. The structure was isomorphous with α-titanium, which is of the space group $P6_3/mmc$ with all the atoms occupying the $\bar{6}m2$ lattice sites. The peak splitting was probably related to the two-phase appearance of the microstructure, indicating that both phases were similar in structure and lattice parameters. At least one of the phases produced superlattice peaks. Based on extinctions (missing peaks) and peak intensities, the superlattice was identified as an $a' = 2a, b' = 2b$ superlattice of the space group $P6_3/mmc$ with the aluminum atoms preferentially occupying the $\bar{6}m2$ lattice sites, and the titanium and niobium atoms randomly occupying the $mm2$ lattice sites.

The oxide of the dynamically exposed specimens was predominantly TiO_2, with Al_2O_3 and TiN

present in lesser quantities, and in specimens with 4 hr or more exposure a trace of Ti_3O_5 was present. In figure 5 the composition of the oxide is shown for exposure times up to 8 hr. The compositions were determined from peak heights in the diffraction spectra, and, considering the assumptions used, the compositions are probably not more accurate than 5 atom percent.

Oxygen Diffusion

Compositional broadening of the (00ℓ)-type peaks was very pronounced after as little as 2.5 min at 982°C, indicating diffusion of oxygen into the base alloy. Composition-depth profiles were calculated from the compositional broadening by assuming that the lattice dilation with oxygen content was the same for this alloy as for α-titanium. The solubility limit of oxygen in Ti-14Al-21Nb appeared to be 12.5 atom percent. In figure 6 the diffusion coefficients are plotted against inverse temperature. The diffusion coefficient for oxygen in Ti-14Al-21Nb was 0.0234 $cm^2/sec \exp\left(\frac{-45\,090\ cal/mole-K}{RT}\right)$ between 704°C and 982°C.

Emittance

The spectral emittance of Ti-14Al-21Nb after various exposures is shown in figure 7; data for oxidized α-titanium is included to demonstrate the expected spectral emittance of a titanium alloy. The spectral emittance of Ti-14Al-21Nb with no oxidation (0 hr exposure) is typical of the spectral emittances of unoxidized metallic surfaces. The spectral emittance of oxidized α-titanium shows the effect of a thin TiO_2 layer on a metallic surface. The spectral emittances of Ti-14Al-21Nb after 0.5 and 1 hr exposures are much higher than for the unoxidized alloy. Knowing that TiO_2 is the predominant oxide that forms on Ti-14Al-21Nb, that TiN is present to some extent in oxidized Ti-14Al-21Nb and oxidized α-titanium, and that Al_2O_3 (present in very small quantities in the oxide of Ti-14Al-21Nb) has a low emittance the high spectral emittances of Ti-14Al-21Nb with 0.5 and 1 hr exposures are unexpected.

The spectral emittance of Ti-14Al-21Nb was high for all exposure times greater than 0 hr. Spalling of the oxide seemed to have no effect. When the top two, loosely adherent oxide layers were removed from a specimen that had 8 hr of exposure, the spectral emittance increased slightly, indicating that the bottom oxide layer was the source of the high emittance. Pieces of the bottom oxide layer were examined with a transmission electron microscope (TEM) equipped with EDS. When the electron beam illuminated a large number of crystals, titanium and niobium were seen (the EDS device was not capable of detecting oxygen). When the electron beam was focused to a convergent beam and centered in the middle of any well-defined crystal, only titanium was seen, indicating that the niobium was not dissolved in the TiO_2. By moving the convergent beam around, the niobium was located in small particles (60 -360 Å in diameter) at the edges of large TiO_2 crystals. The particles did not diffract, so no oxidation or phase information could be obtained. Because these were the only compositional or morphological anomalies observed, the high spectral emittance of Ti-14Al-21Nb was attributed to these niobium-rich particles.

In table IV the total normal emittances of Ti-14Al-21Nb and several other candidate metallic heat shield alloys are presented together. The total normal emittance of Ti-14Al-21Nb is much greater than MA 956 and coated MA 956, and comparable to Inconel 617.

Catalytic Efficiency

Shown in figure 8 are the room temperature catalytic efficiencies of Ti-14Al-21Nb and several other alloys; the catalytic efficiencies were determined from measurements of the heating rates of the different materials at a reference test condition. The curve for aerothermal heating as a function of catalytic efficiency is based on Goulard's solution to the stagnation point laminar boundary layer equations and was used to calculate catalytic efficiencies from heating rates (ref. 1). Silver, which has a high catalytic efficiency and is well documented ($\gamma = 0.25$) (ref. 13), was used as the reference material for characterizing the HYMETS test environment. The observed catalytic efficiency of MA 956 was significantly less than the catalytic efficiency of silver, and the observed catalytic efficiencies of Inconel 617 and Ti-14Al-21Nb were higher than that of MA 956. Under dynamic oxidation conditions, MA 956 and Inconel 617 formed oxides that were predominantly Al_2O_3 and NiO, respectively (ref. 14). A significantly lower catalytic efficiency was measured on coated MA 956; the coating was a boro-alumino-silicate deposited by chemical vapor deposition and was designed to have a low catalytic efficiency (ref. 3). The lowest catalytic efficiency obtained was for polished Ti-14Al-21Nb, which was one-fifth that of coated MA 956.

The catalytic efficiency of Ti-14Al-21Nb on initial exposure to hypersonic test conditions (unoxidized alloy) was significantly lower than for subsequent exposures where the specimen had developed a heavily oxidized surface.

In table V are the high-temperature catalytic efficiencies for Ti-14Al-21Nb and several other alloys. These data are not plotted on a curve similar to that in figure 8 because the HYMETS test environment varied with specimens as their catalytic efficiencies and emittances varied. The HYMETS operating conditions were adjusted to produce a surface temperature of 982°C. All the alloys represented in this figure were represented in the previous figure. All the alloys have catalytic efficiencies similar to their room temperature catalytic efficiencies. A large difference was observed for Ti-14Al-21Nb: its high-temperature catalytic efficiency was nearly that of Inconel 617.

Concluding Remarks

The alloy Ti-14Al-21Nb is highly susceptible to dynamic oxidation, has a high emittance after oxidation, and is fully catalytic to recombination of atomic oxygen under dynamic oxidation conditions at 982°C. Because of its poor oxidation resistance and high catalytic efficiency, use of Ti-14Al-21Nb in certain hypersonic applications will require that it be coated with oxidation barriers and thermal control coatings.

The oxide formed during dynamic oxidation was composed of several layers and spalled during the first half-hour exposure cycle. The phases formed were TiO_2, Al_2O_3, TiN, and Ti_3O_5.

Oxygen diffused rapidly into the alloy. The solubility limit of oxygen in the alloy appeared to be 12.5 atom percent and the diffusion coefficient for oxygen in the alloy was 0.0234 cm^2/sec $\exp\left(\frac{-45\,090\ cal/mole-K}{RT}\right)$ between 704°C and 982°C.

The emittance of Ti-14Al-21Nb was about 0.3 before oxidation and about 0.85 after oxidation. The high emittance of the oxidized alloy was attributed to niobium-rich particles found in the oxide.

NASA Langley Research Center
Hampton, VA 23665-5225
September 18, 1989

References

1. Goulard, R.: On Catalytic Recombination Rates in Hypersonic Stagnation Heat Transfer. *Jet Propuls.*, vol. 28, no. 11, Nov. 1958, pp. 737–745.
2. Schaefer, John W.; Tong, Henry; Clark, Kimble J.; Suchsland, Kurt E.; and Neuner, Gary J.: *Analytic and Experimental Evaluation of Flowing Air Test Conditions for Selected Metallics in a Shuttle TPS Application.* NASA CR–2531, 1975.
3. Clark, Ronald K.; Cunnington, George R., Jr.; and Robinson, John C.: Vapor-Deposited Emittance-Catalysis Coatings for Superalloys in Head-Shield Applications. *J. Thermophys. & Heat Transf.*, vol. 1, no. 1, Jan. 1987, pp. 28–34.
4. Dunkle, R. V.; Edwards, D. K.; Gier, J. T.; Nelson, K. E.; and Roddick, R. D.: Heated Cavity Reflectometer for Angular Reflectance Measurements. *Progress in International Research on Thermodynamic and Transport Properties*, Joseph F. Masi and Donald H. Tsai, eds., American Soc. for Testing and Materials, c.1962, pp. 541–562.
5. Touloukian, Y. S.; and DeWitt, D. P., eds.: *Thermal Radiative Properties—Nonmetallic Solids.* IFI/Plenum, 1972.
6. Anderson, L. A.: Effect of Surface Catalytic Activity on Stagnation Heat-Transfer Rates. *AIAA J.*, vol. 11, no. 5, May 1973, pp. 649–656.
7. Pope, Ronald B.: Stagnation-Point Convective Heat Transfer in Frozen Boundary Layers. *AIAA J.*, vol. 6, no. 4, Apr. 1968, pp. 619–626.
8. Scott, Carl D.: Catalytic Recombination of Nitrogen and Oxygen on High-Temperature Reusable Surface Insulation. AIAA-80-1477, July 1980.
9. Wiedemann, K. E.; Unnam, J.; and Clark, R. K.: Deconvolution of Powder Diffraction Spectra. *Powder Diffr.*, vol. 2, no. 3, Sept. 1987, pp. 130–136.
10. Wiedemann, K. E.; Unnam, J.; and Clark, R. K.: Computer Program for Deconvoluting Powder Diffraction Spectra. *Powder Diffr.*, vol. 2, no. 3, Sept. 1987, pp. 137–145.
11. Wiedemann, K. E.; and Unnam, J.: A Method of Rapidly Obtaining Concentration-Depth Profiles From X-Ray Diffraction. *J. Appl. Phys.*, vol. 58, no. 3, Aug. 1, 1985, pp. 1095–1101.
12. Wiedemann, Karl E.; Unnam, Jalaiah: Rapid Composition-Depth Profiling With X-Ray Diffraction: Theory and Practice. *Advances in X-Ray Analysis*, Volume 29, Charles S. Barrett, Jerome B. Cohen, John Faber, Jr., Ron Jenkins, Donald E. Leyden, John C. Russ, and Paul K. Predecki, eds., Plenum Press, c.1986, pp. 193–202.
13. Wiedemann, K. E.; Shenoy, R. N.; Unnam, J.: Microhardness and Lattice Parameter Calibrations of the Oxygen Solid Solutions of Unalloyed α-Titanium and Ti-6Al-2Sn-4Zr-2Mo. *Metall. Trans.*, vol. 18A, no. 8, Aug. 1987, pp. 1503–1510.
14. Linnett, J. W.; and Marsden, D. G. H.: The Kinetics of the Recombination of Oxygen Atoms at a Glass Surface. *Proc. Royal Soc. London*, ser. A, vol. 234, Mar. 6, 1956, pp. 489–504.

Table I. Chemical Analysis of Ti-14Al-21Nb

Chemical analysis	
Element	Weight percent
Al	14.57
V	.13
Fe	.11
O	.110
C	.04
N	.010
H	.00267
Nb	19.93
Other	<.10
Other total	<.40
Ti	Remainder

Table II. Range of Conditions for HYMETS Exposure

Specimen surface temperature, °C	982
Surface pressure, Pa	530 650
Free-stream Mach number	3.5 3.8
Free-stream enthalpy, MJ/kg	5.30 7.50
Catalytic hot-wall heating rate, kW/sq m	200 290

Table III. Reference Conditions for Cold-Wall Catalytic Efficiency Determination

Catalytic cold-wall heating rate, kW/m^2	408
Free-stream enthalpy, MJ/kg	9.5
Free-stream pressure, Pa	65
Free-stream Mach number	3.8
Surface pressure, Pa	710

Table IV. Total Near-Normal Emittances for Selected Candidate Metallic Heat Shield Alloys and Coatings

Alloy or coating	Total near-normal emittance
Ti-14Al-21Nb	0.88
Inconel 617	.84
MA 956	.67
Coated MA 956	.64

Table V. Catalytic Efficiencies for Selected Candidate Metallic Heat Shield Alloys and Coatings

Alloy or coating	Catalytic efficiency
Ti-14Al-21Nb	0.07
Inconel 617	.083
MA 956	.026
RCG (Shuttle tile coating)	.043
Coated MA 956	.013

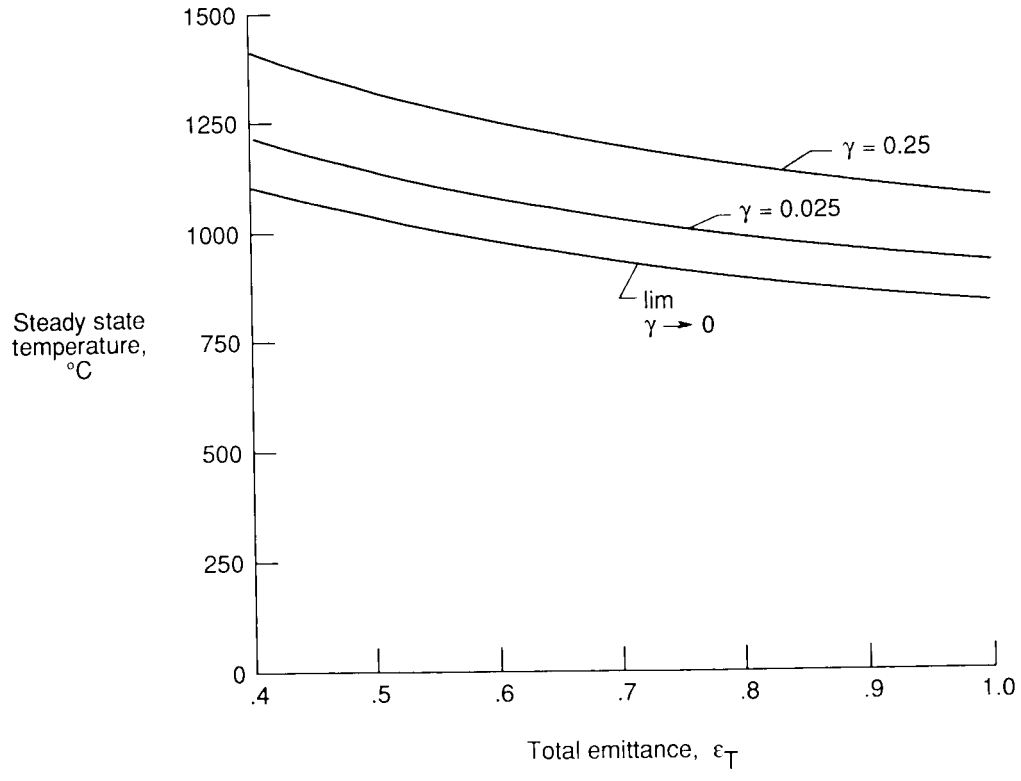

Figure 1. The combined effect of emittance and catalytic efficiency on steady state temperature. $h_{se} = 7.2$ MJ/kg; $T_w = 2995°C$; $p_{se} = 5.4 \times 10^{-3}$ atm; oxygen: 95 percent dissociated; nitrogen: 0 percent dissociated.

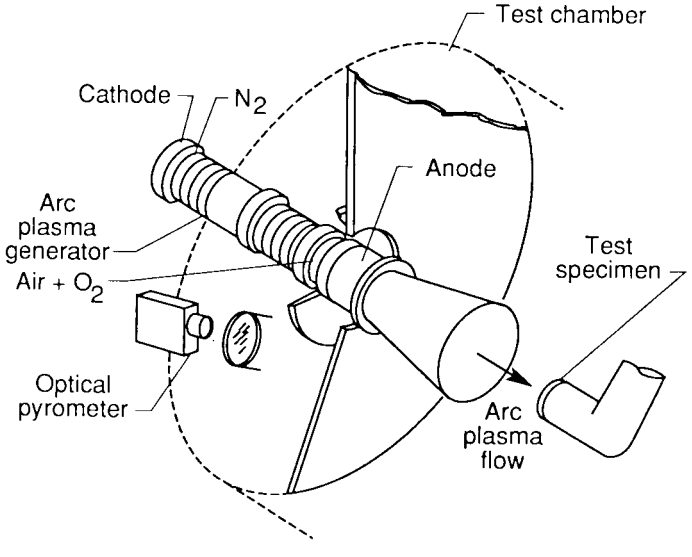

Figure 2. Schematic diagram of the HYMETS facility.

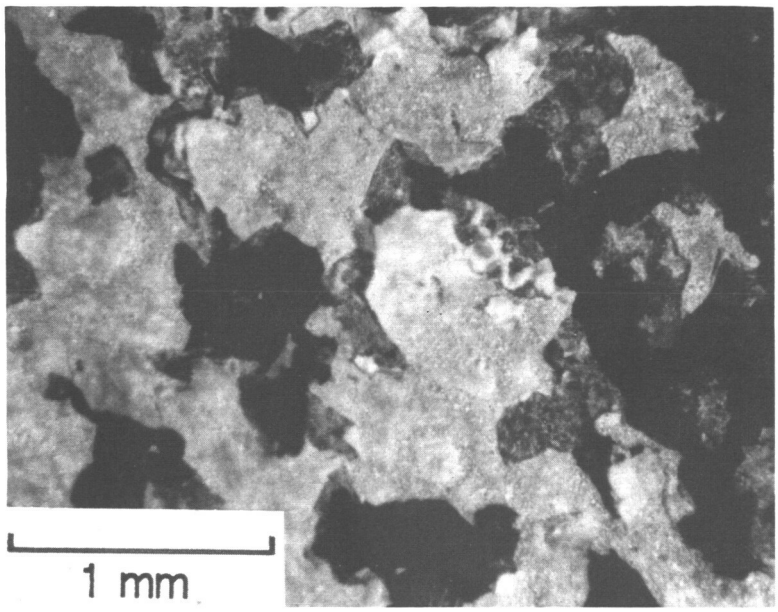

Figure 3. Oxide spalling on a Ti-14Al-21Nb specimen after 8 hr of dynamic exposure at 982°C.

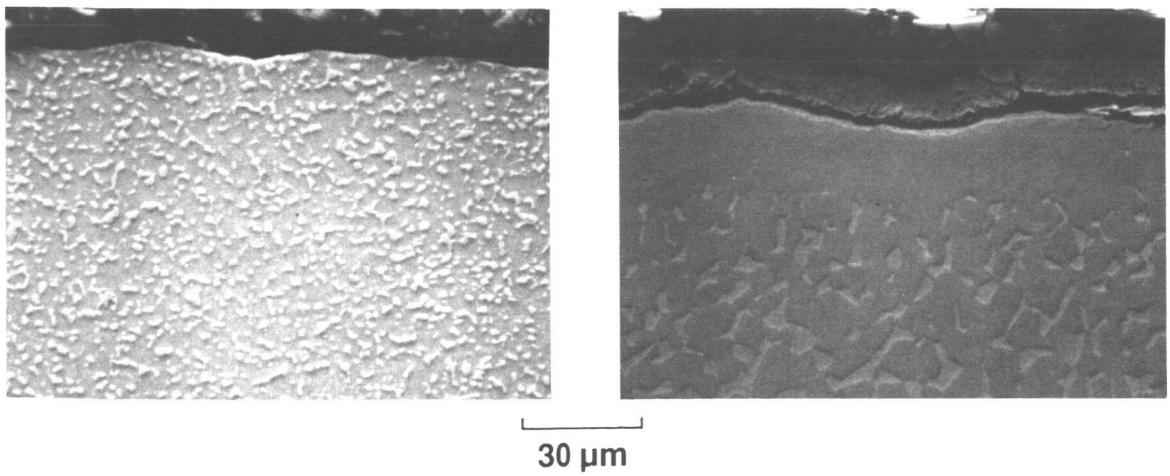

(a) Before exposure. (b) After 8 hr of dynamic exposure at 982°C.

Figure 4. Cross-sectional micrographs of a Ti-14Al-21Nb specimen.

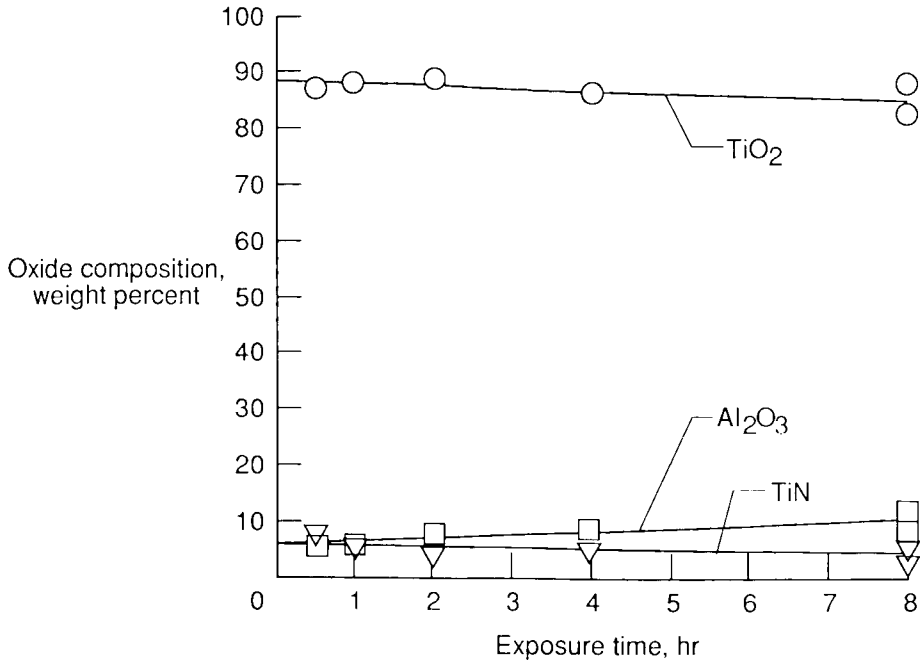

Figure 5. Composition of the oxide scale of Ti-14Al-21Nb specimens after dynamic exposure at 982°C.

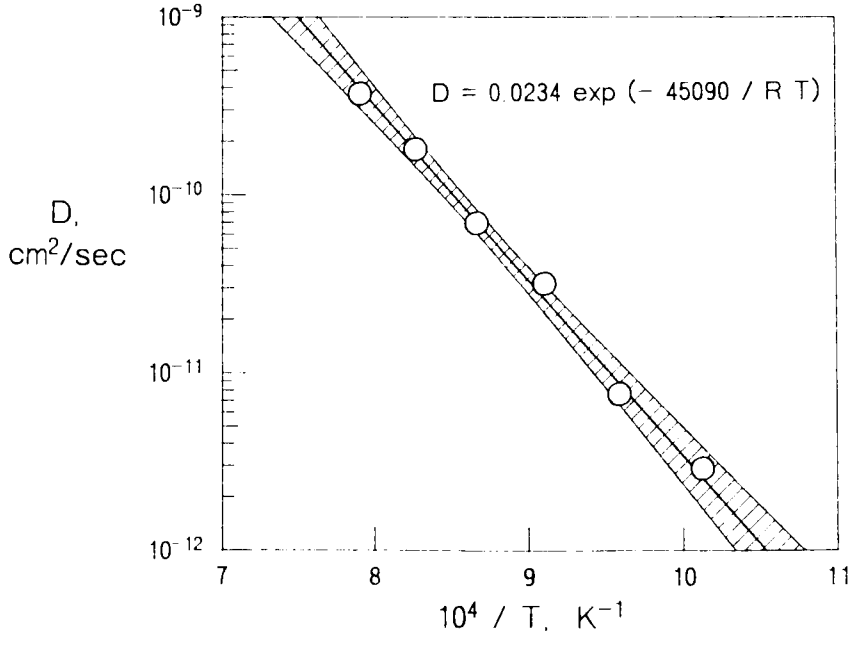

Figure 6. Arrhenius plot of diffusion coefficients for oxygen in Ti-14Al-21Nb from short-time static exposures.

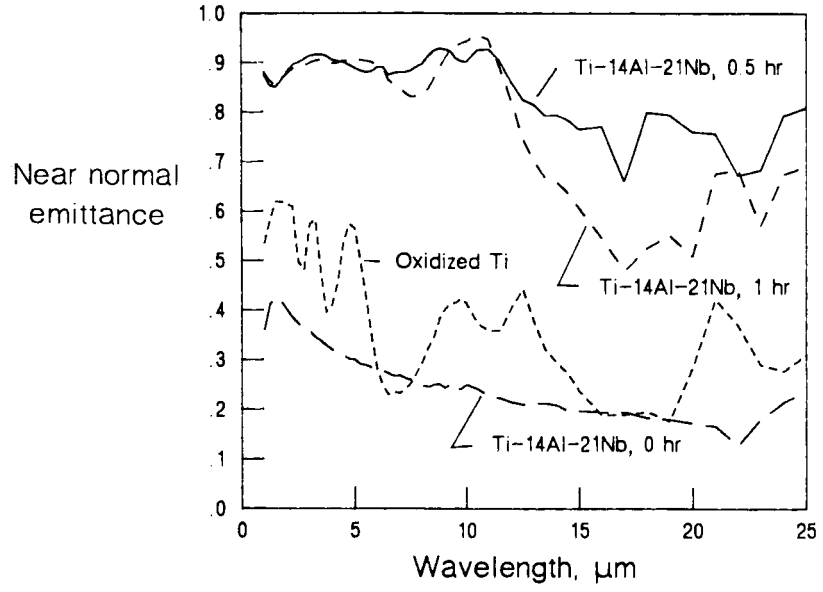

Figure 7. Spectral emittances of Ti-14Al-21Nb specimens after dynamic exposure at 982°C, and the spectral emittance of oxidized α-titanium.

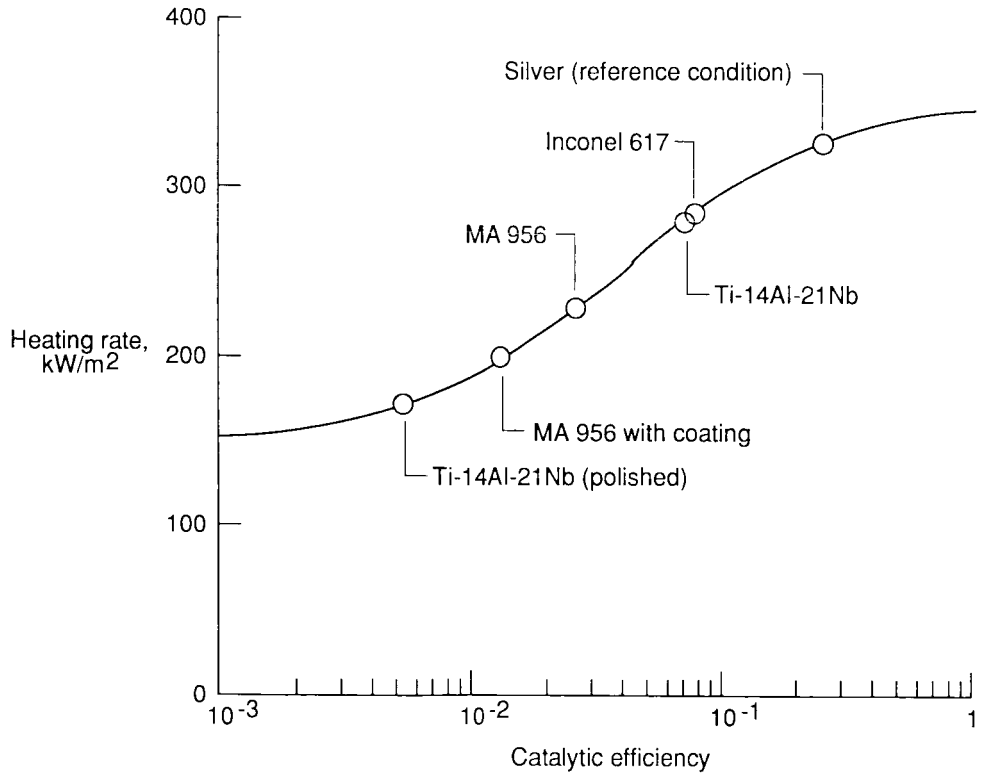

Figure 8. Catalytic efficiencies of Ti-14Al-21Nb and several other materials at 52°C. Mach number = 3.6; Steam enthalpy = 7.2 MJ/kg.

NASA
National Aeronautics and Space Administration

Report Documentation Page

1. Report No.	2. Government Accession No.	3. Recipient's Catalog No.
NASA TP-2955		

4. Title and Subtitle	5. Report Date
Emittance, Catalysis, and Dynamic Oxidation of Ti-14Al-21Nb	November 1989
	6. Performing Organization Code
7. Author(s)	8. Performing Organization Report No.
K. E. Wiedemann, R. K. Clark, and S. N. Sankaran	L-16606
9. Performing Organization Name and Address	10. Work Unit No.
NASA Langley Research Center Hampton, VA 23665-5225	506-43-71-01
	11. Contract or Grant No.
12. Sponsoring Agency Name and Address	13. Type of Report and Period Covered
National Aeronautics and Space Administration Washington, DC 20546-0001	Technical Paper
	14. Sponsoring Agency Code

15. Supplementary Notes

K. E. Wiedemann and S. N. Sankaran: Analytical Services & Materials, Inc., Hampton, Virginia.
R. K. Clark: Langley Research Center, Hampton, Virginia.

Presented at the 1988 Annual Meeting of TMS AIME, January 1988, Phoenix, Arizona.

16. Abstract

Emittance, catalytic efficiency, and dynamic oxidation resistance were determined for Ti-14Al-21Nb exposed to simulated hypersonic flight conditions at a surface temperature of 982°C for up to 8 hr. The emittance was low before testing (about 0.3), but high after testing (0.85 to 0.89). Catalytic efficiencies were high, which means that during exposure to hypersonic conditions Ti-14Al-21Nb will experience a large amount of heating due to recombination of gaseous atoms at the surface. Oxides that formed on the surface spalled readily, beginning with the first exposure cycle. Oxygen diffusion into the base metal was observed. The solubility limit of oxygen in the base metal was 0.0234 $cm^2/sec \exp\left(\frac{-45\,090\ cal/mole-K}{RT}\right)$ between 704°C and 982°C (where R is the universal gas constant and T is the absolute temperature). The oxide was composed of several layers of different color but similar composition: TiO_2, Al_2O_3, TiN, and Ti_3O_5 were identified by X-ray diffraction.

17. Key Words (Suggested by Authors(s))	18. Distribution Statement
Emittance Catalytic heating Oxidation Titanium aluminides Intermetallic alloys	Unclassified Unlimited Subject Category 26

19. Security Classif. (of this report)	20. Security Classif. (of this page)	21. No. of Pages	22. Price
Unclassified	Unclassified	14	A03

For sale by the National Technical Information Service, Springfield, Virginia 22161-2171

National Aeronautics and
Space Administration
Code NTT-4

Washington, D.C.
20546-0001